Comparative Study of the Pulse Shape Discrimination (PSD) Performance of Fast Neutron Detectors

P. A. Kendall, K. Duroe, P. R. Arthur, M. Ellis, M. C. Owen, R. S. Woolf, E.A. Wulf, A. L. Hutcheson, and B. F. Phlips

***Abstract*– Certain scintillating materials are sensitive to both gamma and neutron radiation and can give information about the type of interacting radiation due to differences in the light output response. By collecting the light pulses and converting them to electrical signals the nature of the radiation can be determined by measuring the amount of electrical charge in the pulse tail – for neutrons, the pulses are longer, with more charge in the tail than for the shorter gamma pulses. This determination called Pulse Shape Discrimination (PSD) can nowadays be performed in real-time onboard digitisers during data collection. In this work several detectors (EJ301, EJ309 liquids; EJ299-33 plastic and p-terphenyl scintillators) of various shapes and sizes were connected to several digital Data Acquisition (DAQ) systems as well as the established digital / analogue hybrid Mesytec MPD8 / MADC-32 set up in a comparative study. The aim of the campaign was to produce a Figures of Merit (FOM) for the PSD performance of the various detector / DAQ combinations to give relative performance estimates of the CAEN V1751 10-bit 1 GSample/s digitiser in comparison with other DAQ solutions within a near-standardised experimental environment. It is likely that the DAQ set ups were not equivalent as significant differences in the matching of the detector outputs to the dynamic range of the digitisers were observed – however, with the configurations used in this campaign the CAEN V1751 digitiser showed superior FOM values to the Struck SiS3320, Bridgeport usbBase and Mesytec MPD-8 DAQ systems tested. Furthermore, there seemed little difference between the FOM from the faster but lower voltage resolution (1 GSample/s with 10 bits) CAEN V1751 compared to the slower but higher resolution (250 MSample/s with 12 bits) CAEN N6720 digitiser for this application.**

I. Introduction

CERTAIN types of materials such as liquid scintillators are sensitive to both gamma and neutron radiation. The technique of Pulse Shape Discrimination (PSD) is commonly used, in such detection media, to separate gamma and neutron events. This can be done since light pulses emitted following neutron interactions have longer decay tails than those from gamma interactions [1]. These pulses are typically converted to electrical signals using Photomultiplier Tubes (PMTs) and then fed into a data acquisition system. A common implementation of PSD involves determining the integral charge in the tail ('pulse shape') and the integral of the whole charge pulse, (typically called 'amplitude' or 'energy') of the digitised pulse. For the CAEN DPP-PSD solution the "PSD" parameter is calculated for each digitised pulse as [2]:

$$PSD = \frac{Q_L - Q_S}{Q_L}, \qquad (1)$$

where Q_L and Q_S are the charge contained within a long and short charge integration gate respectively. The resulting PSD and energy values are typically displayed as 2D scatter plots; for a well set up DAQ system the pulses will tend to fall into two overlapping distributions – one with a higher PSD value corresponding to neutrons and a one with a lower PSD value corresponding to gammas, see Fig. 1. In liquid scintillators where a thermal neutron sensitive material has been added (e.g. ^{10}B as with the EJ309 B5 used in this study), thermal neutrons are evidenced by a third distribution between the neutron and gamma distributions at low energies [3].

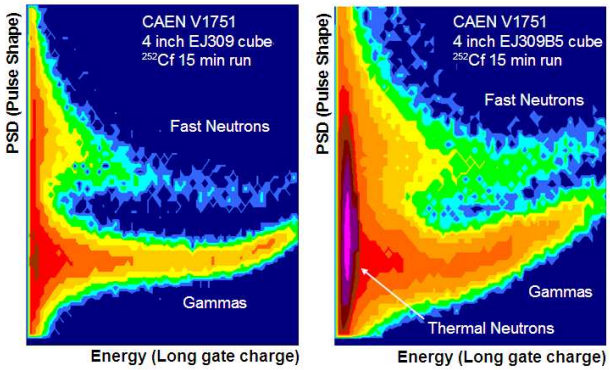

Fig. 1: 2D PSD vs. Energy intensity plots for 4 inch EJ309 and EJ309B5 detectors. Distinct distributions can be seen corresponding to gamma and fast neutron events respectively while a third thermal neutron distribution is seen for the borated detector. Slight curvature is present at high energies due to input saturation.

By projecting this data, summed over a range of energies, onto the 'pulse shape' axis a lineout containing both the neutron and gamma data is obtained. Ideally, the neutron and gamma distributions can be fitted with Gaussian curves. How well the distributions of gammas and neutrons may be separated can be expressed as a unitless figure of merit (FOM) which is the

Manuscript received November 15, 2014. This work is supported by the U.K. Home Office and Ministry of Defence.

The work conducted by NRL co-authors was sponsored by the Chief of Naval Research (CNR).

P. A. Kendall, K. Duroe, P. R. Arthur, M. Ellis and M. C. Owen are with AWE, Aldermaston, Reading, Berkshire RG7 4PR, UK (e-mail: paul.kendall@awe.co.uk)

R. S. Woolf, E. A. Wulf, A. L. Hutcheson, and B. F. Phlips are with the Space Sciences Division, Naval Research Laboratory, Washington DC 20375, USA

978-1-4799-6097-2/14/$31.00 ©2014 IEEE

ratio of the separation of the two Gaussian curves and the sum of their Full Width at Half Maxima (FWHM), Fig. 2 [4].

The PSD FOM is typically evaluated over many lower energy cuts to generate a FOM curve with respect to energy range. Where an energy cut is given, all events below this energy have been removed and the remaining events projected on to the PSD axis to calculate the FOM. Depending on the DAQ solution, curving of the distributions may occur at high energies due to saturation of the input range of the digitiser, resulting in clipped pulses. Where clipping is present a high energy cut may also be introduced to remove clipped events as these can affect FOM values; the effect increases as the low energy cut approaches the energy that corresponds to the maximum unclipped long gate charge.

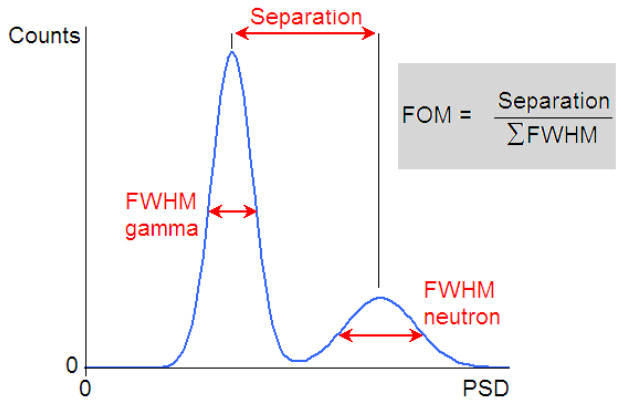

Fig. 2: Illustration of the relevant parameters for calculating the FOM

The PSD performance will depend on many factors – in terms of the detector, the size and geometry have strong effects with smaller, equal-dimensioned geometries giving better PSD as a result of superior light collection (see [5] for an in-depth study of EJ309); for the DAQ, the quality of set up (linear energy calibration, non-curved gamma and neutron distributions) will similarly affect PSD.

The aim of this piece of work was to evaluate the PSD performance of numerous combinations of detectors and DAQ systems with the aim of informing future experiments and design of neutron detection systems.

II. Experimental Set up, Measurements and Analysis

The detector and DAQ systems which were fielded are summarised in Table 1 and Table 2 respectively. All combinations were tested with the exception of the Bridgeport DAQ which was only compatible with the 6" EJ309, the EJ299-33 and the p-terphenyl detectors. To make the best comparison, an experimental set up was used where all eight detectors were fielded in a semi-circular arc equidistant around a central source position, Fig. 3. Large thicknesses of HDPE were used to reduce scattering between detectors.

Table 1: Detector Material and Dimensions

Detector	Material	Dimensions
1	EJ309	102 x 102 x 102 mm (4" cube)
2	EJ309	152 x 152 x 152 mm (6" cube)
3	EJ301	203 x Ø 203 mm (8" cylinder)
4	EJ301	127 x Ø 127 mm (5" cylinder)
5	EJ309-B5	102 x 102 x 102 mm (4" cube)
6	p- terphenyl	76 x Ø 76 mm (3" cylinder)
7	EJ299-33	102 x Ø 102 mm (4" cylinder)
8	EJ309	254 x 254 x 102 mm (10"x10"x4")

Table 2: DAQ solutions and specifications

DAQ	Sampling	Bits	Input Range
CAEN V1751	1GS/s	10	1Vpp
CAEN N6720	250MS/s	12	2Vpp
Struck SiS3320	250MS/s	12	2Vpp
Mesytec MPD8/MADC32	-	-	5Vpp
Bridgeport usbBase	120 MS/s	12	1Vpp

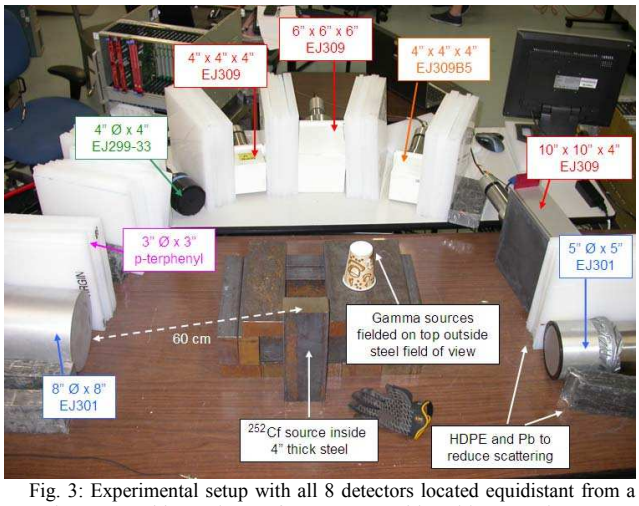

Fig. 3: Experimental setup with all 8 detectors located equidistant from a central source position. Sheets of HDPE are positioned between detectors to reduce cross scattering. The ^{252}Cf source, when used, was placed behind at least 4 inches of steel to reduce the gamma field.

The experiments were undertaken in the middle of a large room to reduce wall scatter of neutrons. Therefore, by using a common source standoff the flux experienced by each detector should be very similar. The set up allowed (depending on the limitations of each DAQ) up to eight detectors to be connected and collecting data at once. Neutrons were from a ^{252}Cf source positioned inside 4 inches of steel shielding to reduce gamma output. Gamma sources for calibration were fielded on a raised low atomic number stand on top of the steel source house (to remove the steel from the field of view). A high activity ^{137}Cs source was also used to test PSD and DAQ data throughput performance at very high input count rates.

The experiments used a variety of detectors that were available but which lacked commonality in terms of component parts such as PMTs. This is not ideal as it introduces additional variables to an already large parameter space; with such differences potentially impacting comparative analysis.

Parameter setting for each detector / DAQ combination was made by using ^{137}Cs and ^{252}Cf sources to optimise the 2D pulse shape vs energy plots with emphasis on separation and straightness of the gamma and neutron distributions. Also performed at this stage was rough gain matching for a given DAQ system (achieved by varying the high voltage applied to the detector) by setting the Compton edge of the gamma distribution to an approximate energy channel number. Calibration was performed by taking data with ^{137}Cs and ^{60}Co sources as well as background data (where the ^{40}K and ^{208}Tl Compton continua were visible).

Following a similar approach as that laid out in [6], the detector response to ^{137}Cs, ^{60}Co and background irradiation was modelled in the Monte Carlo code MCNPx. Gaussian broadening and scaling was then applied to the raw MCNP results to match the spectra from the modelled and experimental data and the resultant Compton edge positions used to generate a calibration curve, Fig. 4.

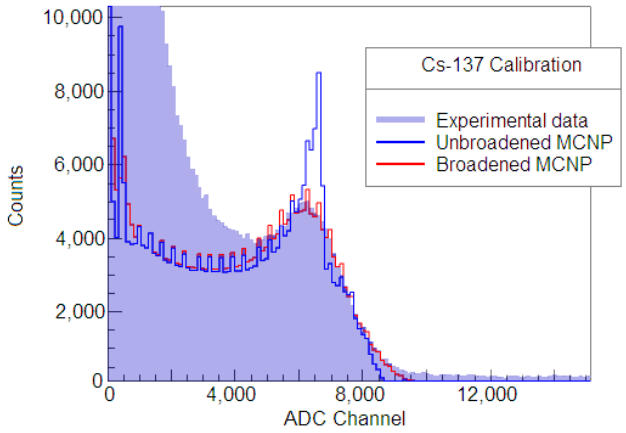

Fig. 4: Compton edge fitting using broadened MCNPx modelling data. MCNPx modelled data (blue) is scaled and normalised to fit experimental data around the region of the Compton edge. The position of the unbroadened Compton edge can then be used to determine the channel to energy relation

The analysis involved: the calibration of the energy scales for each detector with each DAQ system (as detailed above); the conversion of raw binary files into text files; and the calculation of figure of merit values. Independent analysis performed using ROOT / C and using MATLAB provided equivalent answers giving confidence in the quoted results. In both cases the data points falling above a selected lower energy value were projected onto the PSD axis – depending on the curvature of the gamma and neutron lobes within the PSD-energy plot it was sometimes also necessary to enforce an upper limit on energy. Two Gaussian curves were then fitted to the gamma and neutron distributions in the PSD projection to determine the figure of merit. The figure of merit curves were generated by repeating the procedure at a variety of lower energy cuts.

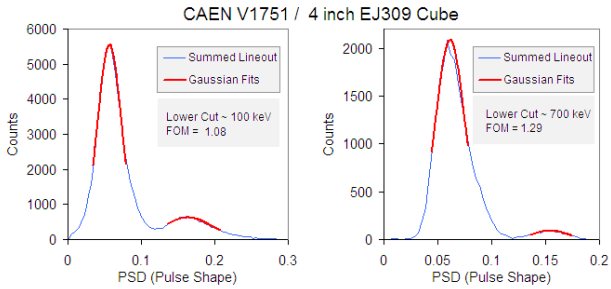

Fig. 5:Example of Gaussian curve fitting, for two low energy cuts, used to calculate FOM values for the 4" EJ309 detector with the CAEN V1751 digitiser.

III. Results

The FOM curves generated for all eight detectors using the CAEN V1751 DAQ are shown in Fig. 6 – the standout performers were the p-terphenyl and 5" EJ301 detectors.

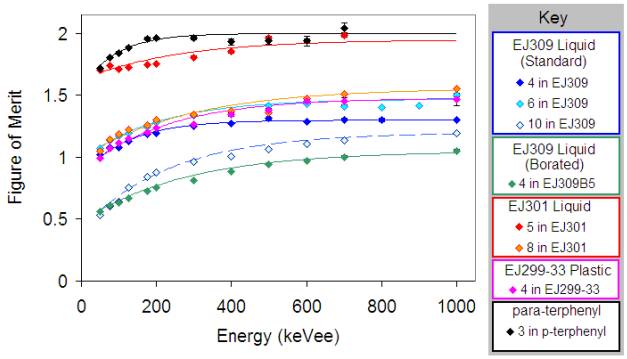

Fig. 6: Comparison of FOM results for the CAEN V1751 digitiser for all detectors

Fig. 7, Fig. 8 and Fig. 9 breakdown the FOM plots for the EJ309 (and EJ309B5) detectors as a function of DAQ system. For the CAEN V1751 (Fig. 7), it can be seen that the 6" detector performs best, then the 4" and finally the 10 x 10 x 4". It is to be expected that smaller detectors will, in general, perform better than larger ones by virtue of better light collection [5]. However, due to the 6" detector having a relatively large PMT, covering ~ 60 % of the detector side compared to ~ 45 % (4") and ~ 17.5 % (10" with a small PMT on one of its 10 x 4" sides), the increase in performance over the 4"detector may be explained. The borated EJ309 B5 has significantly worse FOM – there is a localised hotspot corresponding to thermal neutrons at low energies but the FWHM of the gamma and neutron distributions are poorer anyway. Both the thermal neutron distribution and the wider fast neutron and gamma lobes relative to the same sized EJ309 detector can be seen in Fig. 1.

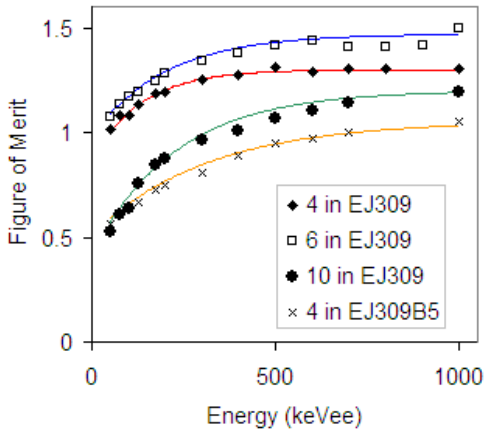

Fig. 7: CAEN V1751 FOM results for EJ309 detectors

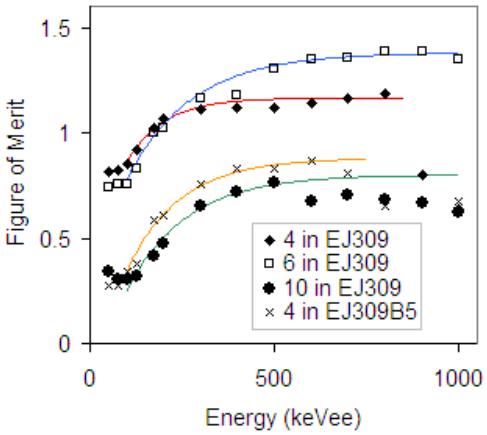

Fig. 8: Struck SiS3320 FOM results for EJ309 detectors

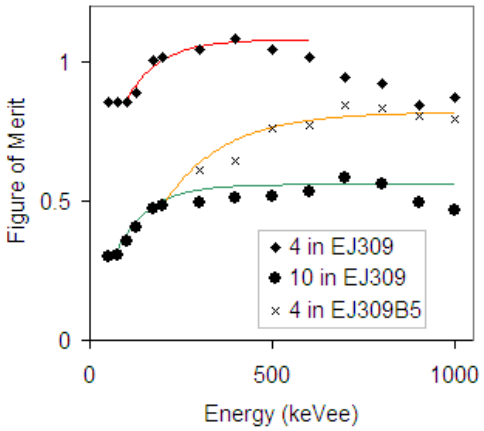

Fig. 9: Mesytec MPD-8 FOM results for EJ309 detectors

It proved impossible to derive FOM values from the 6" detector data collected using the MPD-8 due to severe distortion of the 2D pulse shape-energy plot. The relative performance, within a single DAQ system, of the three EJ309 detectors is mirrored in the SiS3320 and MPD-8 data confirming the detector is responsible, primarily due to the geometry of the material. The performance of the EJ309 10"x10"x4" detector is significantly improved for the V1751 data, with a maximum FOM of around 1.1 compared to 0.7 and 0.6 for the SiS3320 and MPD-8 respectively. The 4" EJ309 data for the MPD-8 data shows a significant degradation in FOM above 600keV not observed with the other DAQ systems. By looking at how the FWHM sum and separation values change with gamma energy (Fig. 10) it can be seen for the 4" detector (red curve) that at higher energies the neutron-gamma separation decreases – for the CAEN V1751 and Struck SiS3320 data the FWHM sum decreases with energy while for the Mesytec MPD-8 this sum remains near-constant. Inserting these trends into the FOM equation yields a drop in FOM for the MPD-8 with increasing energy as seen in Fig. 9. A similar trend is seen for the SiS3320 4" EJ309B5 data at higher energies.

Similarly, referring to Fig. 10 it can be seen that the better relative performance of the 10" EJ309 compared to the 4" EJ309B5 for the V1751 is due to better gamma-neutron separation while the FWHM sums are rather similar. By comparison the 10" values have worse separations for the other two DAQ systems. For the SiS3320, the 10" has a better FWHM sum which offsets the separation and leads to very similar curves in Fig. 8. For the MPD-8 the 10" has higher FWHM sums than the borated detector leading to FOM values that are considerably lower.

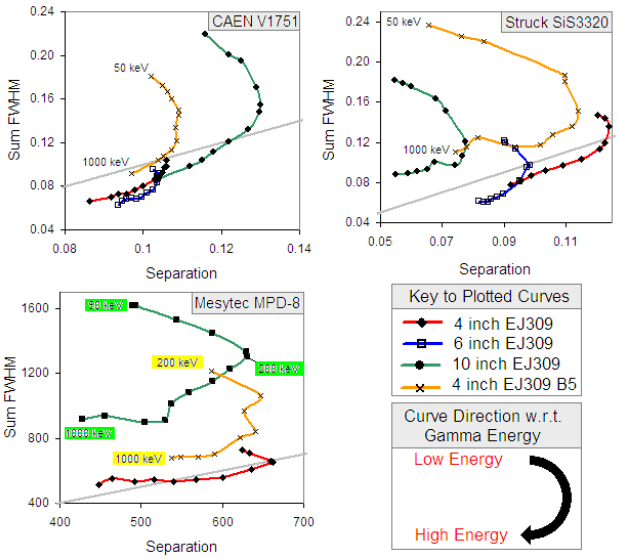

Fig. 10: FWHM Sum vs Peak separation for EJ309 detectors with the various DAQ systems

From Fig. 6 it can be seen that, for the CAEN V1751 data the 5" EJ301 detector significantly outperforms the 8" EJ301 detector – again this is expected to be due to improved light collection and a PMT which covers a greater proportion of the detector surface.

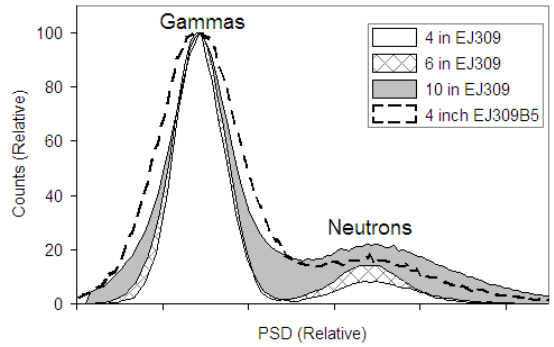

Fig. 11: Comparison of EJ309 detector results projected onto the PSD axis; the count rates have been normalised to the height of the gamma peak rate.

Fig. 11 shows CAEN V1751 PSD data (from 100 to 1500 keVee) for the various EJ309 detectors – the gamma-neutron peak separations for the 4", 6" and 4" borated cubes are rather similar while the 10" detector has better separation. The FWHM of the neutron peak for the 6" detector is slightly smaller than that of the 4" detector which is where the improved FOM arises. The addition of the 5 % boron-loading in the 4" EJ309B5 detector leads to a considerable increase in the magnitude of the FWHM.

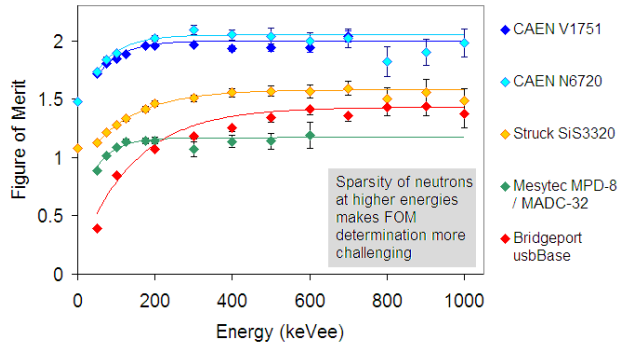

Fig. 12: Comparison of FOM performance for the p-terphenyl detector for a subset of the fielded DAQ systems

A comparison of the FOM performance for the p-terphenyl detector (the only common detector for all the fielded DAQ systems) is given in Fig. 12. An apparent improvement in performance is observed with both of the CAEN DAQ systems, V1751 and N6720, which might not be expected since the N6720 has the same sampling rate, voltage resolution and input voltage range as the SiS3320. This difference in performance was observed for the majority of the fielded detectors although the relative magnitude of the difference varied from detector to detector. The p-terphenyl detector gave the most significant difference in performance and so is presented here.

A significant difference in specification between several of the DAQ systems, summarised in Table 2, is the varying input ranges of the cards. As no amplification was used between the detectors and digitisers the differences in dynamic range will correspond to differences in the sensitive energy range in some cases. 2D PSD vs Energy plots for the p-terphenyl detectors connected to various DAQ systems are shown in Fig. 13.

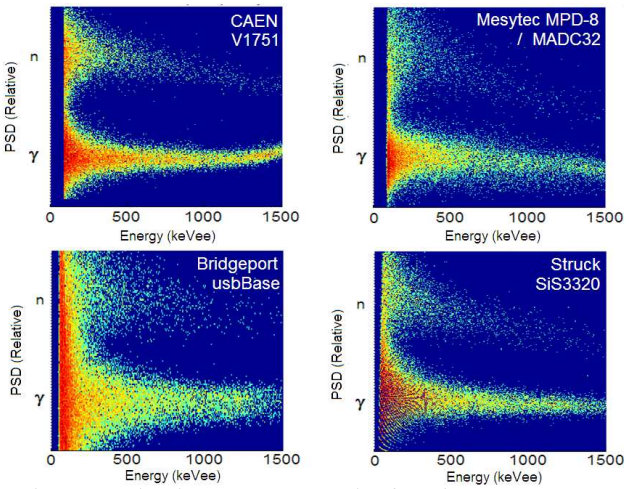

Fig. 13: p-terphenyl PSD vs Energy 2D plots for various DAQ systems

From inspection of 2D PSD vs Energy plots at higher energies for each of the digitisers it can be seen that saturation of the input, indicated by curvature of the PSD distribution, occurs at significantly lower energies for the CAEN digitisers compared to the SiS3320 and MPD-8.

IV. Discussion

By fielding several detectors and DAQ systems in a near-standardised experimental set up, it has been possible to gather comparative PSD data. Due to the number of variables in a rather limited number of detectors this data set has proved suitable to perform broad comparisons of performance versus detector size, geometry, detection medium, etc. For example, EJ301 outperforms EJ309; smaller detectors perform better than larger ones.

A comparison of different DAQ solutions has been attempted but time limitations have prevented a full and systematic optimisation of configuration parameters for each detector and DAQ combination. While some parameters may only have a small impact of the FOM results others such as the matching of the detector output to the dynamic range of the digitiser and the sensitive energy range have been found to significantly affect the FOM performance. As such a definitive comparison of the performance of the fielded DAQ solutions is not possible with this data set.

However information gathered here will be used to inform decision making in future comparative work. The data forms a part of a larger study with smaller subsets of variables being investigated in more focussed studies – for example, the investigation into the effect of geometry and size on EJ309 detectors using a CAEN 1720 digitiser reported previously [5]. Future work will focus on other areas of interest within the multi-variable space. The results from these pieces of work have informed on suitable choices of detector and DAQ to be

fielded in multi-detector fast neutron detector systems under development.

ACKNOWLEDGMENT

The authors wish to thank the UK Home Office and Ministry of Defence for funding this research. Thanks also to the US Chief of Naval Research (CNR) who sponsored the work conducted by the NRL co-authors.

REFERENCES

[1] T. K. Alexander, F. S. Goulding, "An amplitude-insensitive system that distinguishes pulses of different shapes," Nucl. Instrum Meth., vol. 13, pp. 244-246, 1961.

[2] "UM2580 DPSD User Manual", downloaded from www.caen.it

[3] L. Swiderski, M. Moszyński, D. Wolski, J. Iwanowska, T. Szczęśniak, G. Pausch, C. Plettner, J. Stein, P. Schotanus, C. Hurlbut, "Comparison of a neutron detection efficiency using a He-3 counter and a Boron-10 loaded liquid scintillator EJ309B5", IEEE Nucl. Sci. Symp. (2009) N24-190

[4] G. F. Knoll, "Radiation Detection and Measurement (4th Edition)", Wiley

[5] M. Ellis, C. Tintori, P. Schotanus, K. Duroe, P. A. Kendall, and G. Mini, IEEE Nucl. Sci. Symp. (2013) N20-1

[6] Ashrafi S., and Ghahremani Gol M., Nucl. Instrum Meth A, vol. 642, pp. 70-74, 2011